Proceedings of ASME Turbo Expo 2023
Turbomachinery Technical Conference and Exposition
GT2023
June 26-30, 2023, Boston, Massachusetts, USA

GT2023-104145

OPTIMIZING MICRO GAS TURBINE OPERATION IN A MICROGRID SYSTEM WITH NATURAL GAS AND HYDROGEN FUEL: AN AI-BASED APPROACH

Reyhaneh Banihabib — University of Stavanger, Stavanger, Norway
Fredrik Skaug Fadnes — Norconsult AS, Oslo, Norway
Mohsen Assadi — University of Stavanger, Stavanger, Norway
Boris Bensmann — Leibniz University Hannover, Hanover, Germany

ABSTRACT

In the coming years, decentralized power generation systems with renewables are expected to take a leading role, and micro gas turbines will serve as backup sources to compensate for times of low inputs from other sources. In order to deal with the unpredictable energy inputs from renewables, the micro gas turbine must be capable of running under varying load conditions and making fast transitions between them.

The operation of a micro gas turbine in an integrated microgrid has the potential to reduce operational costs and ensure the delivery of demanded heat and power to consumers. This paper investigates the operation of a micro gas turbine in a microgrid, serving as a supplementary power source for a municipal building. The building's required energy is initially provided by wind turbine power, and the micro gas turbine serves as a backup source during times of wind power deficiency. The micro gas turbine can operate using a natural gas/hydrogen fuel blend ranging from zero to 100% hydrogen. Furthermore, a water electrolyzer with a hydrogen tank is available to operate as a storage system within the microgrid. The study's results demonstrate the economic and environmental benefits of using hydrogen storage and optimizing operational planning in the microgrid. The primary objective of the paper is to highlight the feasibility and benefits of employing micro gas turbines and hydrogen storage systems within a microgrid as a renewable energy backup power source.

Keywords: Microgrid, micro gas turbine, hydrogen storage, hydrogen-enriched fuel, operation optimization, AI, Data-driven.

NOMENCLATURE

Alphanumeric Variables

C	Cost (EUR)
D	Direction (deg)
Inc	Incentive (EUR)
LHV	Lower heating value (kJ/kg)
$\dot{m}$	Mass flow rate (g/s)
n	Number of hours in the window of optimization
P	Power (kW or MW)
p	Pressure (Pa)
Pen	Penalty (EUR)
pr	Price (EUR)
Q	Heat exchange (MW)
R	Revenue (EUR)
S	Speed (m/s)
T	Temperature (K)
t	Time (s)
V	Valve position (%)
X	Optimization parameters series

Greek Symbols

η	efficiency

Indices

amb	Ambient
dem	Demand
eg	Exhaust gas
el	Electricity
f	Fuel
mnt	Maintenance
opt	Optimum
W	wind

Abbreviations

AI	Artificial intelligence
ANN	Artificial neural network
CL	Catalyst layers
DEM	Demand
ELZ	Electrolyzer
FR	Fuel ratio
GE	Grid export
GI	Grid import
HE	Heat exchanger
MAE	Mean absolute error

ME	Maximum error
MG	Microgrid
MGT	Micro gas turbine
MSE	Mean squared error
NG	Natural gas
PEM	Proton exchange membrane
PTL	Porous transport layers
PV	Photovoltaic
TOT	Turbine outlet temperature
WT	Wind turbine

1. INTRODUCTION

The global energy demand is increasing with the growing population and urbanization which will result in high CO_2 emissions if the power generation scheme does not shift away from fossil fuel-dependent technologies [1]. The consequences of carbon-based emissions are warmer climates with extreme weather events such as a dryer climate in one region and more floods in others [2], sea level rise, and vegetation changes. Other than global warming consequences, the emissions are associated with air pollution which also has destructive effects on living beings [3].

The power generation sector is accountable for a considerable share of CO_2 emissions. Power generation is responsible for 33 billion tonnes of CO_2 production in 2019 which was 77% of the whole emissions that year [4]. In fact, finding cost-efficient solutions to decarbonize power generation is one of the biggest challenges of the EU energy sector. Energy transition, i.e. the replacement of fossil fuel-based power producers with low-carbon or carbon-free resources has been enforced by international climate policies [5]. The energy transition leads to a paradigm shift from production in centralized power plants to a decentralized generation of renewables in distributed locations. In this transformation, the governing forces (regulations, policy implementations, and incentives) emphasized the importance of efficiency, flexibility, and reliability [6]. These concerns require improved grids with higher efficiency of production, more flexibility in operation, and low chances of interruptions. The microgrid concept is the consequence of such drives [7].

A collection of interconnected power and heat resources and consumers located in close proximity to a defined electrical boundary form a microgrid (MG) [7]. MGs are able to operate independently from the traditional grid when the demanded power and heat by the consumers (residential, industrial, etc.) are supplied by different types of sources available inside the MG, i.e., island mode. MG could also connect to the grid and import or export power from other MGs i.e., grid mode [8].

In the island mode, the MG is isolated from the sources outside of its boundary, and is therefore controlled by a system independent from the grid [9]. The management of power and heat generation inside a microgrid is dependent on the enclosed resources, however, in case of surplus or deficiency, power could be transferred through the point of common coupling, the connection point of the microgrid to the grid.

MGs offer efficiency and flexibility as the production depends on localized heat and electricity generation systems, such as solar PV, solar thermal, wind turbines, small hydro turbines, etc. [10]. The development of dispatchable generators is also directed towards small-scale units, gas-fired with an option to use both fossil fuels as well as environmentally friendly alternatives such as bio-fuels, ammonia, hydrogen, etc. A micro gas turbine is a small-scale turbine with a power rate below 300 kW that could be driven by a variety of fuels to cogenerate electricity and heat. Their quick load-following and flexibility of operation in a range of power rates from minimum load to full-load condition make them an advantageous choice as a dispatchable backup unit inside a renewable-based microgrid.

Another backup strategy for the microgrid is the storage concept that could save the surplus power for the time of deficiencies in the grid. Storage technologies and backup generators are necessary for a microgrid to maintain a reliable operation and prevent failures [11]. Storage refers to the conversion of electrical energy to potential energy in different forms such as chemical, mechanical, electrical, electrochemical, and thermal [10]. Power-to-Hydrogen is one way of power storage in chemical form, where renewable energy is used for the electrolysis of water to produce hydrogen. In this case, a generator unit that is capable of running with the stored hydrogen fuel for power (and/or heat) production should be present inside the MG as well.

Changing the power production paradigm from a centralized scheme to a decentralized form could increase the reliability of the power generation system. The dependency of a large number of consumers on a single power plant (centralized), will transform into a smaller group of consumers depending on various types and numbers of generators, i.e. decentralized. Microgrids are able to isolate the failing part of the system from the rest and rely on other generators and assure uninterrupted operation [7]. As the flexibility of MG operation is increased due to the various technologies in the system, managing the operation becomes increasingly intricate. The non-dispatchable units of MGs' dependency on the ambient conditions (weather) bring significant challenges to the power management system. The small size of the distributed generators and the lack of control over their power production may lead to episodes of insufficient production as well as oversupply.

Intelligent management of MG operation enhances the power quality in an MG through proper control of the generators. Optimizing the control and operational schedule of MGs has been pursued by researchers, aiming for lower operational costs, maintenance costs, and environmental impacts of the MG. A systematic overview of the literature on the optimization of the energy management system of microgrids in island mode has been provided in [12]. Optimization with different approaches in terms of time-frame, optimization objectives, and employed optimization methods are categorized [12]. The authors of reference [13] suggest the use of artificial intelligence (AI) to address the challenges of distributed energy generation and microgrid systems. They introduce a simulation framework and identify relevant data sources that can facilitate the development

of AI capabilities in utility systems. Despite the difference in the methods, the common approach for the studies is to provide a representative model of the microgrid and search for an optimized operational strategy by evaluating the model's reaction to different operational strategies.

A microgrid model consists of integrated models of the subsystems, i.e., the generator and consumer units inside the MG. The accuracy of subsystems' model prediction and its ability to capture the operational traits, especially during load transitions has a significant effect on the reliability of the method and the outcomes. A common approach for microgrid modeling is to represent the subsystems with simplified polynomial regression models [14], [15]. To increase the accuracy of the subsystems' performance predictions, physics-informed models have been employed by researchers, usually using modeling software such as SIMULINK. The efforts made throughout the current work were to increase the fidelity of the microgrid model by employing AI that could provide highly accurate predictions. In this approach, data collected from actual subsystems (wind turbine, micro gas turbine, etc.) is used for training a model, so it fits best with the data and will be able to provide predictions. A data-based model does not incorporate physical correlations, unlike a physics-based model. However, the data used to train the model contains information about the physics of the subsystem, which can be inferred by the trained model [16]–[18].

Utilization of AI-based tools is beneficial for micro-grid optimization purposes for several reasons:

- Accuracy: with simplified correlations or even elaborated physics-based models, deviations of model predictions from outcomes of the actual element is expected. In such cases, an elaborated adaptation of the physics-based model to real components will be required which is a time-consuming task [19].
- Prediction speed: for optimization purposes, an iterative procedure will be conducted to search for an optimized control strategy. Therefore, employing a high-speed model has a significant advantage, especially when operational planning for a close future is intended.
- The AI-based models provide the possibility of online condition monitoring for an asset. Giving highly accurate predictions, the deviations of the model and the system outputs at any point of MG operation could be realized as degradation or fault in the system. This is beneficial in two regards: for small deviations, a quick refit of the model to the data will update the model to the new system and therefore maintain the performance of the optimization algorithm. For high rates of deviation with the chance of shutdowns, the model could be employed to estimate the time of failing and prevent abrupt stops. Also, the system could be rapidly updated to pursue optimized operation without the faulty subsystem. Such a condition monitoring system facilitates maintaining the microgrid and lowers costs [20].
- A data-based approach is also beneficial when data accessibility is provided between microgrids. The operational strategy and microgrid performance from one system could be useful for others, by AI-interpreted operational guidelines. In other words, the experience with one system could be useful for another one, and an efficient way to convey the information is to provide a shared database which AI-based models could benefit from [20].

In the following sections, a description of the MG system studied is provided and the developed model is presented. The MG is operated with different scenarios, with and without storage and the outcomes of different operations are discussed.

2. SYSTEM DESCRIPTION

An autonomous MG system composed of a wind turbine, a water electrolyzer, and a micro gas turbine is assumed in this work. The heat and power generated in the MG are to satisfy the demand for a municipal office building. Power from wind turbines is the main source to satisfy the needs of the consumer and the micro gas turbine running with natural gas/hydrogen blended fuels works as the backup system.

FIGURE 1 illustrates the schematic view of the MG with the fuel lines, electricity line, and heat line. The direction of transfer through these lines is demonstrated with arrows close to each subsystem. The electricity line is connected to the grid outside of the MG boundary, where the electricity could be imported to or exported from the MG. The MG operation is controlled by an energy management system where the satisfaction of consumer demands is the primary goal.

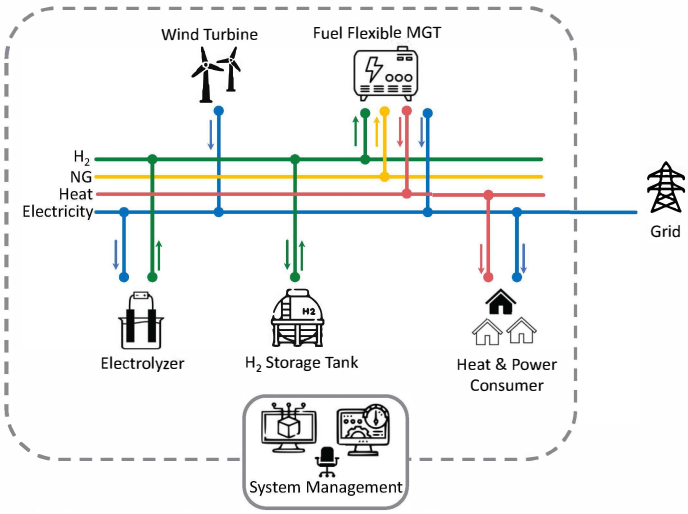

FIGURE 1: SCHEMATIC REPRESENTATION OF THE MICROGRID CASE STUDY.

In this system, the combination of the electrolyzer and H_2 storage tank work as a storage system, where the excess power generated could be used to generate hydrogen and store it in a tank. The hydrogen could be later used for heat and power generation by driving the MGT unit. All components of this microgrid have a specific operational behavior with dependency on various features. For instance, wind turbine operation is dependent on ambient conditions, especially wind speed. The

micro gas turbine's operation is also dependent on the environment, but the power output is controlled by the operator. An accurate model for each of these subsystems is required to enable the simulation and techno-economic optimization of the microgrid.

3. MICROGRID MODEL DEVELOPMENT

The MG model consists of data-driven models for each subsystem shown in FIGURE 1, except for the consumer. The consumer's heat and power demands are imported to the microgrid model as tabulated data. For other subsystems, i.e., the wind turbine, the micro gas turbine and the electrolyzer, AI-based models based on operational data are constructed. The chosen approach for modeling the subsystem is artificial neural networks (ANN).

ANN have proven to be a powerful tool for modeling complicated physical systems [21]. ANN is comprised of connected layers of nodes called artificial neurons. The simplest structure of neural networks is layers of fully connected neurons, in which each neuron of a layer is connected to all of the neurons of the previous layer. Every connection line is an indicator of value transmitted while multiplied by a weight. Inside an artificial neuron, all weighted inputs are summarized and passed as input to a function called the activation function. The output of the neuron is the output of the activation function, which can be a linear or nonlinear form. In FIGURE 2 (A), the structure of an artificial neuron is depicted. The inputs (x) are from the upstream neurons (located at the upstream layer). Other than the inputs from the upstream layer, a bias term (b) is added to the summation of inputs, which is been shown to improve the performance of ANNs. The Bias term has a value of unity and is also multiplied by a weight. In FIGURE 2 (A), w_i is the weight associate with each input, b is the bias term and f is the activation function.

The simplest ANN model consists of two layers, one input layer and one output layer. By adding layers in between (called hidden layers) the model becomes more complicated and at the same time more flexible to imitate complex physical systems. As an example, FIGURE 2 (B) shows a multilayer perceptron with two hidden layers. There are 8 neurons in the first hidden layer and 6 in the second. The network has four inputs and two outputs which impose the number of neurons in the input and output layers.

After identifying the physical system's input and outputs, which will be model's inputs and outputs, the data is sorted as independent variables (inputs) and targets (outputs). Building an ANN model for physical systems begins with choosing a configuration (number of layers, number of neurons, activation functions) for the model that suits the physical system, in terms of the ability to capture complex system behavior. Then, the training begins which includes optimizing all the weights in ANN so that feed-forwarding the independent variables to the trained model gives the results in the last layer that are very close to the targets of the system. For all ANN models in this study, 80% of the whole data was used for training and the remaining 20% was used to verify the performance of the model.

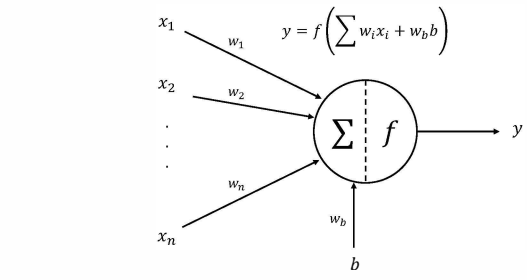

(A)

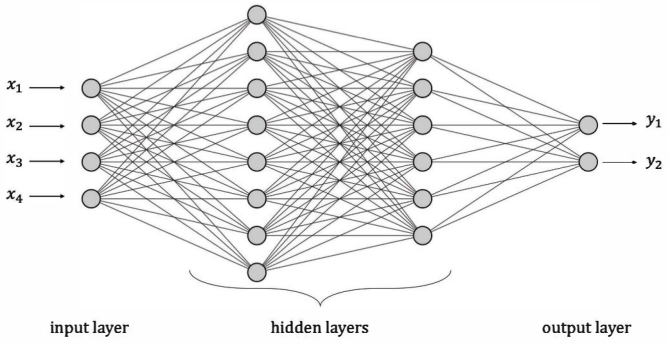

(B)

FIGURE 2: STRUCTURE OF (A) AN ARTIFICIAL NEURON AND (B) A MULTILAYER PERCEPTRON.

The following section provides a description of the subsystems along with the chosen configuration for those with an ANN model. Prediction accuracy evaluation is also presented. The models are based on 80% of real operational data, and their performance is validated using the remaining 20%. The high accuracy of the models, derived from real operational data, ensures the reliability of the microgrid model.

In ANN models, hyperparameters are used to control the behavior of the algorithm, training process, and model structure. Examples include learning rate, number of hidden layers, and activation functions. To achieve optimal performance, hyperparameters are either set through prior knowledge or by searching over a range of values. Hyperparameter tuning can be done manually or through automated methods, such as Bayesian optimization, which involves building a probabilistic model of the function to be optimized and refining it as objective function evaluations are gathered. This method is highly efficient for solving complex and costly optimization problems. in the current work, hyperparameters for every ANN model constructed were derived from performing Bayesian optimization.

3.1 Heat and Power Consumer

The microgrid demand is based on operational demand data from a municipal building located in Stavanger, Norway. The building houses the main city public pool on the ground floor, and the municipal administration is located on floors 1 – 3. The building was equipped with several new electric and thermal energy meters during refurbishment in 2017-2019. The research group responsible for this work has been given access to all operational data in the building.

Historical data for electricity and heat consumption as input to the microgrid was captured at a five-minute time interval. The selected electricity meter measured the complete consumption of the building, except for the electricity used in the operation of the building's thermal energy production system. Thus, the electric demand in the microgrid simulation is not directly coupled with the heat demand.

The heat consumption data was measured at a thermal meter in the thermal distribution system. The building houses an advanced thermal energy plant, which was established as part of the EU lighthouse project Triangulum [22]. Thus, the building has already been an objective of the research, and the investigation of a microgrid operation will provide the municipal energy department with a relevant perspective on advanced modeling and optimization methods.

In the simulated MG, the heating system of the building is represented by a waterborne distribution system primarily heated from the micro gas turbine heat exchanger. Additionally, an electric boiler is set as the peak load and backup unit for heating the water. The efficiency of the boiler is set constant to 85%, taken from the Norwegian Standard for the calculation of the energy performance of buildings [23]. Data for heat and power demand is resampled and total demand per hour is provided, and together with ambient condition data is delivered to the microgrid model in a tabulated format. The ambient condition is prepared as averaged values over each hour. Data from fuel and electricity market (price of electricity and natural gas) is also imported to the model as tabulated data.

3.2 Wind Turbine

The wind turbine power comes from two WTN250 units installed nominal output of 250 kW [24]. Turbine output and ambient conditions were measured at the Norwegian meteorological institute (MET) station 44560 at Stavanger airport Sola, which included the hourly estimations of power production. The model was built based on 10 full years of recorded data for wind speed and direction, from 2007-2016. From the power curve of the wind turbine shown in FIGURE 3, the cut-in wind speed for the selected turbine is 4 m/s, while the cut-off speed is 25 m/s. The maximum rated capacity of the production is reached at 14 -15 m/s, which is 250 kW.

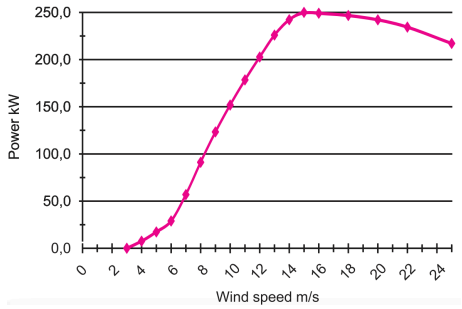

FIGURE 3: WTN 250 POWER CURVE [24].

The ANN model constructed for the wind turbine includes ambient temperature (T_{amb}), ambient pressure (p_{amb}), wind speed (S_W), and wind direction (D_w) as inputs and produced power (P_{WT}) as an output. The configuration of the ANN model with three hidden layers and an overview of the errors are provided in TABLE 1. FIGURE 4 presents a comparison between a month of operational data and the model's predictions, indicating the precision of the model. The Adadelta optimizer and a learning rate of 0.57 are used to train the model.

TABLE 1: CONFIGURATION AND ERROR OF ANN FOR THE WIND TURBINE.

ANN Configuration		ANN prediction Error	
inputs	T_{amb}, p_{amb}, S_W, D_W	ME	27.2
outputs	P_{WT}	MAE	6.67
No. of neurons hidden layers	[45,100,22]	MSE	11.35
Activation function hidden layers	[selu,relu,linear]		

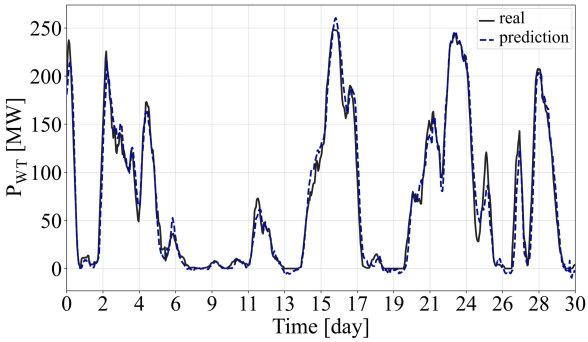

FIGURE 4: WIND TURBINE PERFORMANCE PREDICTION IN COMPARISON TO REAL DATA.

3.3 Fuel-flexible Micro Gas Turbine

The micro gas turbine implemented in the microgrid is a heat and power co-generator unit, running with blended natural gas/hydrogen fuel. The original engine was a commercial Turbec T100 (T100PH), which was redeveloped to enable operations with hydrogen blended fuels. To this end, the fuel train system, combustion chamber, and controller were modified to provide stable operation of the unit in the full range of power output and the full range of hydrogen/methane blend [25].

T100 micro gas turbine is a single-shaft engine with a single-stage compressor, single-stage turbine, and one tubular combustor. The engine generates power through a regenerative Brayton cycle where the excess heat from the turbine leaving gas is used for preheating the air entering the combustor via a recuperator. The hot gas leaving the recuperator is still warm enough to warm up recirculating water for district heating purposes. Therefore, a water-gas heat exchanger (HE) is installed at the bottom of the cycle, where the warm gas leaving the recuperator enters it. The amount of gas entering the heat exchanger is controlled by a valve (HE valve); at a fully open position whole gas flow passes the heat exchanger and in close condition, it bypasses the heat exchanger and discharges to air.

The engine is equipped with a high-speed permanent magnet generator which enables the operation of the engine with variable rotational speed. When the operator sets a demand power, the controller sets the rotational speed and fuel flow rate to meet the demanded power while keeping the turbine outlet temperature (TOT) below and close to a certain value. Running the MGT with almost constant TOT, which is close to its maximum allowed value, protects the hot components (combustor, turbine, and

recuperator) from damage. Moreover, the turbine inlet temperature will remain close to its maximum value which is beneficial for cycle efficiency.

During the redevelopment process of the MGT to enable hydrogen injection, the original fuel delivery system was replaced by a new fuel supply and a new fuel train. An additional controller is employed to operate beside the engine governor. The flow rate of each fuel type is controlled by the fuel train controller, which regulates the valves based on the fuel ratio demanded by the engine operator. Methane and hydrogen enter a mixing station and then, the well-mixed fuel is divided into main and pilot valves controlled by the governor. The operation of the governor is also modified to accommodate a full range of natural gas/hydrogen mixtures [25]. The modified engine and fuel system is shown in FIGURE 5.

The ANN model of the MGT has 3 hidden layers, with demanded power (P_{dem}), fuel ratio (FR), and ambient temperature (Tamb) as input and fuel flow rate ($\dot{m}_f$) and exhaust gas temperature (T_{eg}) as the outputs. The inputs and outputs of the model have been chosen based on the real engine's inputs and outputs. The configuration of the trained model and prediction errors are provided in TABLE 2. The Adadelta optimizer was utilized with a learning rate of 0.82 to train the model. A comparison between actual operation data for two hours and model predictions is provided in FIGURE 6 and FIGURE 7. The temperature of the exhaust gas is used for calculating the heating capacity of the heat exchanger.

FIGURE 5: TURBEC T100 UNIT WITH MODIFIED COMBUSTOR AND FUEL TRAIN FOR FLEXIBLE FUEL OPERATION [25].

TABLE 2: CONFIGURATION AND ERROR OF ANN FOR THE MICRO GAS TURBINE.

ANN Configuration		ANN prediction Error	
inputs	$P_{MGT,dem}$, FR, T_{amb}	ME - $\dot{m}_f$	2.3
outputs	$\dot{m}_f$, T_{eg}	MAE - $\dot{m}_f$	0.14
No. of neurons hidden layers	[36,65,59]	MSE - $\dot{m}_f$	0.38
Activation function hidden layers	[sigmoid,tanh,selu]	ME - T_{eg}	24.0
		MAE - T_{eg}	7.4
		MSE - T_{eg}	11.9

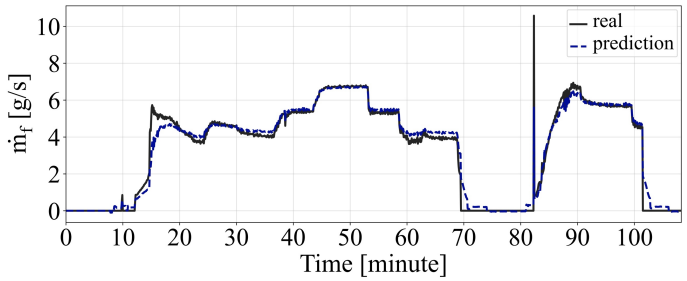

FIGURE 6: MICRO GAS TURBINE FUEL FLOW RATE PREDICTION IN COMPARISON TO REAL DATA.

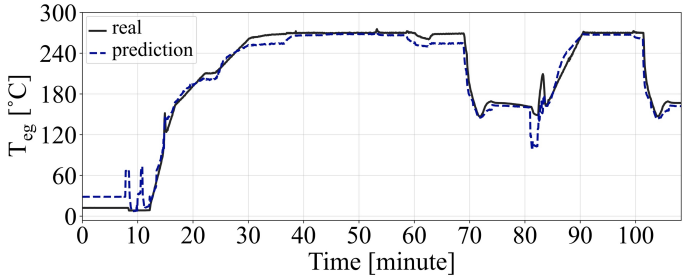

FIGURE 7: MICRO GAS TURBINE EXHAUST GAS TEMPERATURE PREDICTION IN COMPARISON TO REAL DATA.

3.4 Electrolyzer

The electrolyzer is constructed based on a stack of cells shown in FIGURE 8. In the middle of the cell, a proton-conducting membrane serves as the electrolyte. Additionally, it separates the two half-cells. The catalyst layers (CL) follow on both sides. Within those the half-cell reactions take place:

Anode:

$$2H_2O \rightarrow 4H^+ + 4e^- + O_2 \quad (1)$$

Cathode:

$$4H^+ + 4e^- \rightarrow 2H_2 \quad (2)$$

Total:

$$2H_2O \rightarrow 2H_2 + O_2 \quad (3)$$

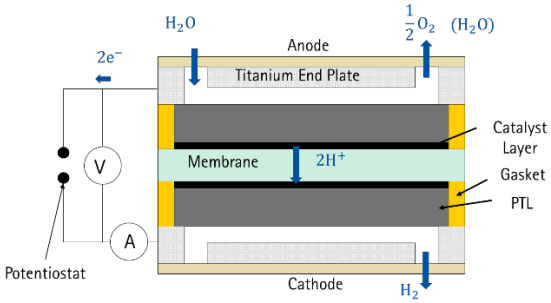

FIGURE 8: TYPICAL PEM-WATER ELECTROLYSIS SETUP FOR ELECTROCHEMICAL WATER SPLITTING.

A commercially available catalyst-coated membrane based on Nafion 212 was assembled in the cell. For the anode side, a porous transport layer (PTL) made of sintered titanium fibers was ultra-sonicated for 10 min in de-ionized water before usage. A carbon paper with hydrophobic treatment was used as the cathode PTL.

Anode PTLs are made from Titanium, cathode side is normally carbon-based. Those serve as the electric contact between end plates and CLs and transport the reactants to and from the CL. Finally, the end plates provide the required clamping pressure and can be equipped with flow channels for better fluid transport.

The electrolyzer model developed in this study is based on scaled-up data from a singular cell designed by Fraunhofer ISE [26], specialized for lab tests with equipment/material for proton exchange membrane (PEM) electrolyzers. The collectors and flow fields are made of gold-coated titanium. The contact force is applied with an adjusting screw perpendicular to the cell's base area and is monitored with a load cell between the screw and the cell. The applied force after thermal conditioning for a single cell unit was 2,5 kN. For means of isolation and proper positioning of both PTLs, each electrode block is equipped with a frame made of polyetheretherketone.

The ANN model built for the electrolyzer is described together with the prediction error assessments in TABLE 3 which predicts the rate of hydrogen production ($\dot{m}_{H_2}$) based on the power consumption inside the electrolyzer (P_{ELZ}). The training process of the model utilizes the Adamax optimizer and a learning rate of 0.05. In FIGURE 9 the power and hydrogen production rate from electrolyzer's operation and model prediction is presented.

TABLE 3: CONFIGURATION AND ERROR OF ANN FOR THE ELECTROLYZER.

ANN Configuration		ANN prediction Error	
inputs	P_{ELZ}	ME	6.0e-4
outputs	$\dot{m}_{H_2}$	MAE	7.1e-7
No. of neurons hidden layers	[98,9,59]	MSE	1.9e-6
Activation function hidden layers	[selu,elu,linear]		

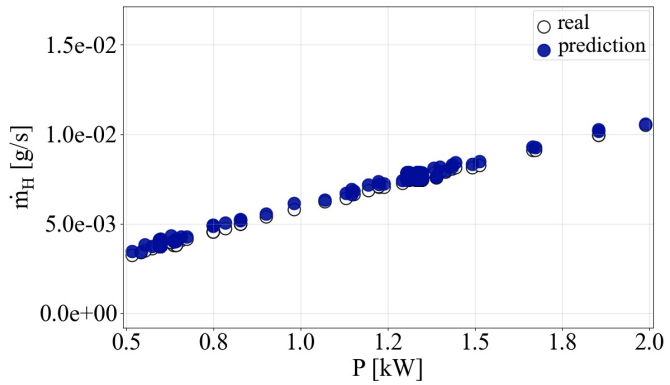

FIGURE 9: ELECTROLIZER PERFORMANCE PREDICTION IN COMPARISON TO REAL DATA.

4. MICROGRID OPERATION OPTIMIZATION

The management system of the MG is in charge of controlling the power and heat source(s) with volatile power inputs and different dynamic behaviors, in order to provide energy for consumers which also has a non-constant demand profile. A smart management system controls the operation of dispatchable units to maintain a reliable source for consumers with an economically beneficial approach. In this section, two operational strategies for the dispatchable units inside the MG are discussed: one, following rules based on the condition of demand and renewable supply units (called condition-based), and another using an optimization algorithm. Both approaches use demands, weather, and price data that are assumed to be available from forecasting for the next 24 hours [27]. The data used in this study, however, is actual data from the dates and hours of the study case.

4.1 Condition-based Operation

In the case of energy management without any optimization involved, a condition-based operation scenario is followed, which focuses on the power and heat balance during each time step. This operational scenario works as follows:

- If wind production is higher than the electrical demand, the remaining power ($P_1 = P_{WT} - P_{DEM}$) is utilized in electrolysis:
  - If P_1 is higher than the electrolyzer's capacity, the remaining power ($P_2 = P_{WT} - P_{DEM} - P_{ELZ}$) will be used for heat generation.
    - If P_2 is higher than the demanded heat, it is exported to the grid.
    - If P_2 is lower than the demanded heat, power is imported from the grid for heating purposes.
- If wind production is lower than the demand, then the micro gas turbine is used to compensate for power.
  - If the remaining power demand ($P_3 = P_{DEM} - P_{MGT}$) is higher than the micro gas turbine's capacity, then power is imported from the grid for power purposes.
  - If the heat produced by the micro gas turbine is lower than the heat demand, power is imported from the grid for heating purposes.

When running the micro gas turbine, the combination of the fuel mixture is based on the highest value of hydrogen available, and the positioning of the HE valve is based on the heat demand. The condition-based scenario is illustrated in a diagram shown in FIGURE 10.

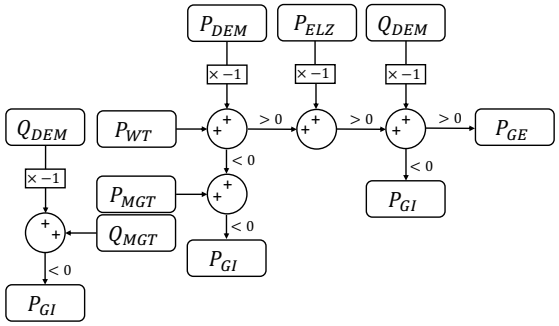

FIGURE 10: CONDITION-BASED OPERATION SCENARIO.

The microgrid operates to provide power and heat to meet the demand within the grid. In situations where there is a deficit of either power or heat, the microgrid imports electricity from the larger grid. The cost of electricity to import is variable, based on the date and the hour of the day. On the other hand, in case of

surplus power, the electricity will be exported to the grid and sold with a value close to the spot price, according to the energy regulatory authority of Norway [28].

4.2 Optimization of MG operation

To determine the optimized performance of the microgrid in the course of one day, hourly data has been utilized and the operation command is provided on an hourly basis as well. Weather data (including pressure, temperature, wind speed, and wind direction), as well as electricity price data, is provided on an hourly basis. The price data for natural gas is provided which changes on a daily basis. The goal of optimization is to operate the dispatchable units of the MG in a manner that together with non-dispatchable inputs, satisfies the heat and power demand in the most economically efficient way. The wind turbine is the only non-dispatchable unit, while the micro gas turbine and electrolyzer are the dispatchable units of the current MG. The optimization parameters are MG power over 24 hours (24 number of parameters, Eq.4), the fuel ratio of the micro gas turbine over 24 hours (24 number of parameters, Eq.5), and the electrolyzer power 24 hours (24 number of parameters, Eq.6). The optimization parameter series X contains all control variables over the course of the management time span (Eq.7). The control parameters are confined between maximum and minimum values, determined by the capacity of each subsystem.

$$P_{MGT} = [P_{MGT_1}, P_{MGT_2}, \dots, P_{MGT_n}], \quad P_{MGT_{min}} < P_{MGT_i} < P_{MGT_{max}} \tag{4}$$

$$FR_{MGT} = [FR_{MGT_1}, FR_{MGT_2}, \dots, FR_{MGT_n}], \quad FR_{MGT_{min}} < FR_{MGT_i} < FR_{MGT_{max}} \tag{5}$$

$$P_{ELZ} = [P_{ELZ_1}, P_{ELZ_2}, \dots, P_{ELZ_n}], \quad P_{ELZ_{min}} < P_{ELZ_i} < P_{ELZ_{max}} \tag{6}$$

$$X = [P_{MGT}, FR_{MGT}, P_{ELZ}] \tag{7}$$

The weather condition is read at each time step (1 hour) and the ANN model for the wind turbines is used to determine their power output. The power and output of the micro gas turbine and the power consumption of the electrolyzer are also calculated based on the respective models of each unit and the inputs from X. The heat production from the micro gas turbine is regulated by choosing the HE valve position. Then, the balance of heat and power is assessed, to determine the value of power to be transferred through the microgrid boundaries.

The cost of operation to minimize includes the cost of MGT and electrolyzer operation. There is a maintenance cost associated with wind turbine operation as well, however, in this study, the wind turbine is assumed to be always running (in times of windy weather) and therefore it does not have a controllable cost to minimize. The cost of maintaining the electrolyzer is also neglected due to its low value compared to its operational cost. The cost of electrolyzer's operation is included in the power allocated to it at each time step.

Micro gas turbine operation cost includes fuel cost and the cost associated with maintenance, as stated in Eq. 8. The cost of natural gas consumption is correlated with the daily price of the fuel (Eq. 9) and the maintenance cost is the effect of the operation on the lifetime of the micro gas turbine which is correlated with the power output over the time of operation (Eq. 10) according to the reference [29]. In Eq. 10, $C_{MGT,mnt,y}$ is the annual maintenance cost of the micro gas turbine per kJ of power production, and Δt is the time step which is 1 hour in this study.

At the beginning of the operation, the amount of hydrogen available is assumed to be zero and for the MGT to operate with hydrogen in a time step, it is necessary that hydrogen was produced by the electrolyzer in previous time steps of that week. Since the hydrogen used as a fuel was produced via the electrolyzer, the cost of its production is already considered in the electrolyzer's power consumption, therefore the MGT fuel cost is reduced to natural gas cost.

$$C_{MGT} = C_{NG} + C_{MGT,mnt} \tag{8}$$

$$C_{NG} = \dot{m}_{NG} \times LHV_{NG} \times pr_{NG} \times \Delta t \tag{9}$$

$$C_{MGT,mnt} = C_{MGT,mnt,y} \times P_i \times \Delta t \tag{10}$$

After balancing the heat and power, the cost of imported electricity from the grid in case of deficiency or the revenue from exporting electricity to the grid in case of overproduction, is calculated via Eq. 11 and Eq. 12 based on the hourly electricity price data per kJ.

$$C_{P_{GI}} = pr_{el,buy} \times P_{GI} \times \Delta t \tag{11}$$

$$R_{P_{GI}} = pr_{el,sell} \times P_{GE} \times \Delta t \tag{12}$$

The optimization process seeks for a set of inputs to the microgrid that reduces its operational cost. The cost of operation includes the cost of running the subsystems plus the cost of electricity imported from the grid, minus the revenue from exporting the electricity to the grid. The objective function of the optimization is shown in Eq. 13. Other than the costs and revenues, an incentive term is subtracted from the objective function to direct the optimizer to more favorable results. This term is correlated with the amount of hydrogen remaining in the tank at the end of the course of operation. The optimization searches for the optimum input series that results in the minimum of the objective function.

$$X_{opt} = \text{argmin}\left(\sum_{i=1}^{n}\left(C_{MGT,i} + C_{P_{GI,i}} - R_{P_{GE,i}}\right) - Inc\right) \tag{13}$$

The reason behind the hydrogen reserving incentive is that when the optimizer is focusing on a specific time span, (e.g., 24 hours) it will aim for reducing the cost within the same time span. Therefore, it is possible that the hydrogen produced during the day will be consumed during the same day. This is still beneficial, both economically and environmentally. For instance, if there is high wind power and low demand in the first half of a day and low wind power and high demand in the second half, the optimizer will find the best solution as producing and saving hydrogen in the first half and consuming it in the second. If the hydrogen content is more than enough for the demand, then it will be used for exporting the excess power to the grid in exchange for the selling price.

Moving on to the next day, the hydrogen tank will be empty and if the day begins with high demands and low wind power inputs, the cost of MGT operation will be higher and if required, power should be imported at the expense of electricity bidding

price. Looking at two consecutive days might lead to the conclusion that saving hydrogen from one day to another could be beneficial. The definite decision could only be made if the data (ambient, demand, and prices) was available for two days, which is unlikely, and even it was possible, then the relation between the first two days with the next two days will become an issue. Therefore, an acceptable approach could be to pursue the optimization within the chosen time span and direct the optimizer to save some hydrogen for the next time span.

In this study, the time span of the optimization is one day but the whole investigation time is a week of operation, and the incentive is useful for saving hydrogen from one day to the next. The hydrogen saving incentive is calculated based on Eq. 14. In this correlation, the worth of hydrogen is calculated based on the potential power output from the MGT using the hydrogen fuel. The price calculation is based on the power production from running the MGT with the reserved hydrogen and $\overline{\eta}_{MGT}$ is the mean efficiency of the MGT from minimum to maximum load. The electricity price is from the last hour of the same day of optimization (as the best guess), since the data from day 2 is unknown when the optimization for day 1 is under process. In fact, all tabular data is made available for 24 hours, and the next 24-hour data will be available at the end of the current day.

$$\mathrm{Inc} = \mathrm{m}_{\mathrm{f,H_2}} \times \mathrm{LHV}_{\mathrm{H_2}} \times \overline{\eta}_{\mathrm{MGT}} \times \mathrm{pr}_{\mathrm{el,sell}} \tag{14}$$

The optimization process with the objective function described is pursed with a constraint, that is also related to the hydrogen tank. The amount of hydrogen consumed at each time step is confined to the amount of hydrogen available.

$$\left(\dot{\mathrm{m}}_{\mathrm{f,H_2}} \times \Delta \mathrm{t}\right)_{\mathrm{i}} \leq \left(\mathrm{m}_{\mathrm{H_2,tank}}\right)_{\mathrm{i}} \tag{15}$$

The amount of hydrogen present in the tank at any given step is determined by the initial content of the tank and the changes in it over the previous steps. These changes are determined by the operational strategy in the previous steps, which involves the production of hydrogen (related to the power of the electrolyzer (Eq. 6) and the consumption of hydrogen (related to MGT power and fuel ratio, Eq. 4, and Eq. 5). Therefore, the controlling parameters at each time step and their degree of freedom are confined by the control parameters in previous time steps, which adds complexity to the optimization process:

$$\begin{aligned}\left(\mathrm{m}_{\mathrm{H_2,tank}}\right)_{\mathrm{i}} = \mathrm{f}(&\left(\mathrm{m}_{\mathrm{H_2,tank}}\right)_{\mathrm{t=0}}, \left(\mathrm{P}_{\mathrm{ELZ}}\right)_{\Delta \mathrm{t=0\sim i-1}}, \\ &\left(\mathrm{P}_{\mathrm{MGT}}\right)_{\mathrm{t=0\sim i-1}}, \left(\mathrm{FR}_{\mathrm{MGT}}\right)_{\mathrm{t=0\sim i-1}})\end{aligned} \tag{16}$$

The methodology presented here allows for the operation optimization of various configurations of MGs, with different subsystems. If operational data from a subsystem were available, a data-based model could be built based on it and easily implemented in the process of performance analysis and optimization. In this paper, the prepared MG optimization code is utilized for the MG configuration presented in FIGURE 1, in two cases of electrolyzer running and shutdown.

5. RESULTS AND DISCUSSION

The data available for the demands of the consumer was limited to 28 weeks, from the 13th of May to the 24th of November 2022. To investigate the performance of the optimizer on a week of MG operation, first, an assessment of the price condition of the 28 weeks is conducted. Based on the authors' experience, the performance of the optimizer improves as the difference between natural gas and electricity price grows. This is because of the micro gas turbine's capability to convert chemical energy to electricity, i.e., MGT's operation makes a profit by converting cheap energy to an expensive one. While the optimizer identifies the price difference and takes advantage of the price situation, the condition-based scenario operates with no regard to the prices, and therefore, the difference between condition-based operation and optimized operation increases as the price difference grows.

Therefore, the week of study was chosen to have a price difference between natural gas and electricity close to the average, to avoid over or underestimation of the performance of the optimizer. According to FIGURE 11, week 10 has an El-NG price difference close to the median value throughout the 28 weeks, with a maximum at week 16 and a minimum at week 27. Therefore, investigating the optimizer's performance on week 10 will give results that are not optimistic or pessimistic.

The ambient conditions over the course of the week are provided in FIGURE 12, FIGURE 13 and FIGURE 14. These conditions have an impact on the power and heat demand as well as the wind turbine power output. Moreover, the ambient pressure and temperature affect the performance of the micro gas turbine; although the MGT provides the power that was demanded (almost), the fuel flow rate and exhaust temperature could be affected by ambient temperature. Variations in fuel flow rate have an impact on the cost of operation and the turbine exhaust temperature affects the capacity of heat production. Therefore, the ambient condition data is provided on hourly bases and imported into the modeling module. All ambient data is extracted from Norwegian meteorological institute (MET) station 44560 at Stavanger airport Sola.

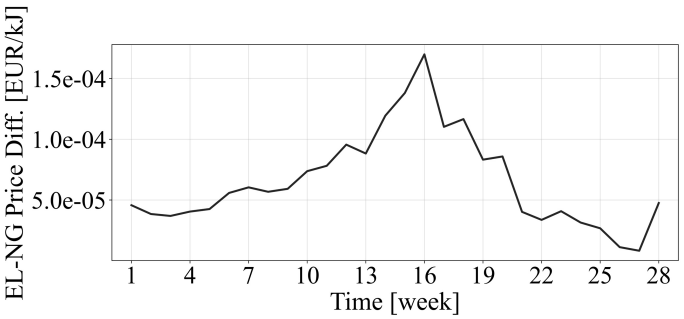

FIGURE 11: DIFFERENCE BETWEEN ELECTRICITY PRICES (SELL) AND NATURAL GAS PRICES FOR 28 WEEKS.

The total value of demanded power, demanded heat, and produced power by the wind turbine for each day is presented in FIGURE 15. As it is shown, the amount of wind turbine power production on days 2 and 7 exceeds the demanded power, and on day 7 exceeds the combined amount of heat and power. However, these are aggregated values; on hourly bases periods of power demand exceeding the wind power supply could be expected during these days.

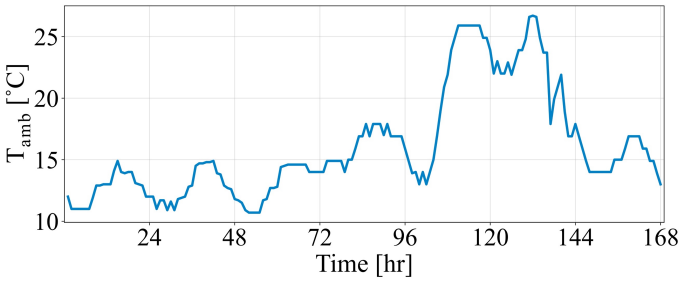

FIGURE 12: AMBIENT TEMPERATURE OVER THE WEEK OF STUDY

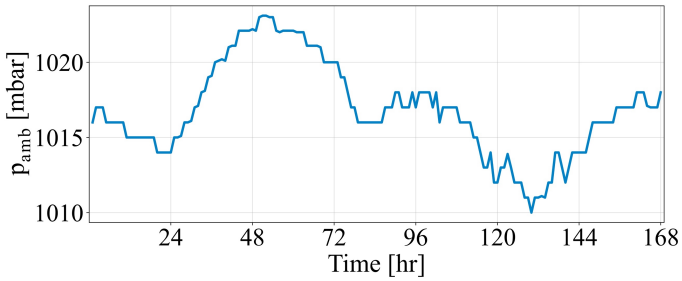

FIGURE 13: AMBIENT PRESSURE OVER THE WEEK OF STUDY

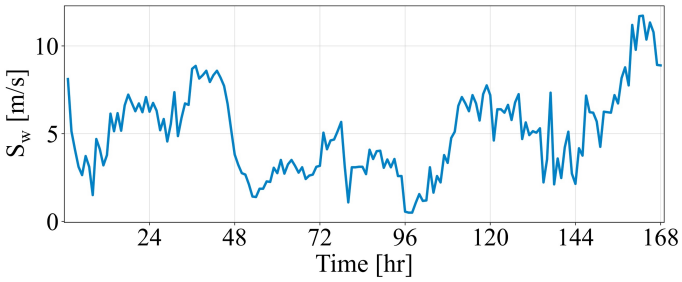

FIGURE 14: WIND SPEED OVER THE WEEK OF STUDY

The relationship between ambient conditions and heat and power demand can be observed by comparing FIGURE 12 to FIGURE 15. As the weather gets colder, the heat and demand increase, therefore beginning days of the week have higher demands compared to day 6 when the temperature is maximum. Moreover, the high wind speed during days 2 and 7 (FIGURE 14) resulted in high wind turbine power production (FIGURE 15).

The investigation for week 10 with both operation scenarios (condition-based and optimization) were pursued. At the beginning of the week, times slot was chosen for optimization, which required 24×3 number of variables to optimize the performance of the MG for a day (Eq. 7). The amount of available hydrogen on day one is set to zero, and when the optimized operation for day 1 is achieved, the amount of hydrogen left from production and consumption of day 1 is transferred to the next day. This is continued until the last day of the week. The optimizer attempts to find the best combination of the parameters distributed over 24 hours. Along with optimization, the condition-based operation is performed and provided for each day, with the same initial condition (zero amount of hydrogen available).

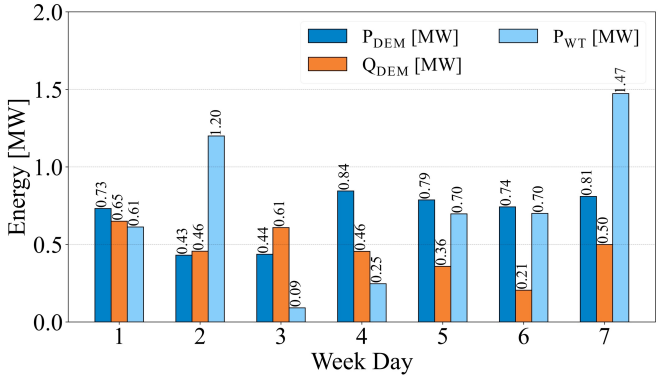

FIGURE 15: POWER AND HEAT DEMAND AND WIND TURBINE PRODUCTION OVER THE WEEK OF STUDY.

Genetic algorithm was implemented for the optimization of the MG performance using SciPy differential evolution toolbox [30]. Genetic algorithm is an optimization method that is inspired by the process of natural selection and evolution. It uses techniques such as mutation and crossover to generate new solutions from existing ones. Unlike traditional optimization techniques, such as gradient descent, genetic algorithms can explore a much larger search space and can explore multiple local optima at the same time and find the global optimum. The goal of a genetic algorithm is to find optimal or near-optimal solutions to complex problems by mimicking the process of natural selection. The average time consumed for optimizing the operation of each day was about 15 minutes, which gave a total of less than 2 hours of optimization time for the whole week. This fast optimization was due to the fact that the modeling module has a very short response time thanks to the data-driven models utilized.

To realize the effect of hydrogen storage in the microgrid, the study was conducted in two cases, one with the configuration suggested in FIGURE 1, and another case with removing the electrolyzer and the hydrogen tank from the microgrid, leaving the system with a wind turbine and a micro gas turbine running on natural gas.

To discuss the results, first, an overview of the cost and revenue of the two MG configurations, for condition-based operation and optimized operation is provided in TABLE 4. The results show how optimized operation improves the economical outcome of the operation. In the case of the electrolyzer involved, 57 percent of the loss is saved by reducing from 170 EUR to 73 EUR by the optimizer. In MG without the electrolyzer, the optimizer reduced the loss from 141 EUR to 82 EUR which equals 42% savings. Moreover, the electrolyzer and hydrogen storage saved about 11 % from loss, reducing 82 EUR to 73 EUR in optimized scenarios.

TABLE 4: COST OVERVIEW OF OPERATIONAL SCENARIOS OVER THE WEEK.

	Condition-based Operation			Optimized Operation		
Case	Cost [EUR]	Rev. [EUR]	Loss [EUR]	Cost [EUR]	Rev. [EUR]	Loss [EUR]
MG w ELZ	170.12	0.00	-170.12	135.48	62.25	-73.23
MG w/o ELZ	173.56	32.52	-141.04	148.48	66.55	-81.93

Assessment of financial state of the operation in daily bases is provided in FIGURE 16. The first observation is that on all days of the week, the optimizer improved the economic performance of the MG compared to the condition-based scenario, whether by lowering the loss or increasing the profit. Moreover, on all days of the week, the microgrid configuration with the electrolyzer performs equally or better than the microgrid without the electrolyzer in optimized operation. However, the condition-based scenario seems to work better without the electrolyzer than with the electrolyzer involved. This indicates that saving all surplus energy from wind will not assure economically beneficial results.

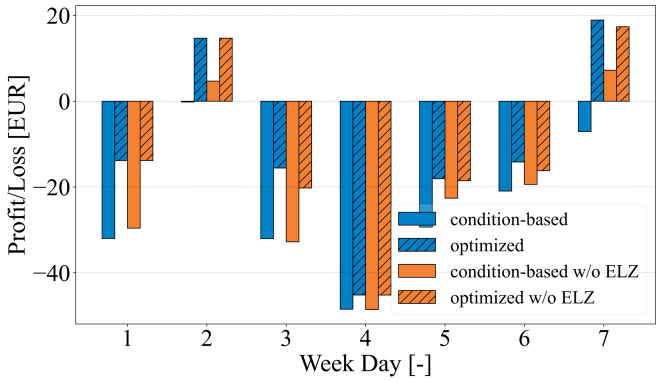

FIGURE 16: PROFIT AND LOSS EVALUATION OVER THE WEEK.

On the other hand, from FIGURE 17 displaying the daily hydrogen consumption, it appears that the condition-based scenario may have generated and consumed a greater quantity of hydrogen, potentially resulting in a more eco-friendly solution. At first, it seems that the condition-based operation has a significant advantage over the optimized case, in terms of hydrogen consumption, which also means that more hydrogen was produced by the electrolyzer the day(s) before. However, a look at FIGURE 18 reveals that micro gas turbine's power production in condition-based operation was higher that of the optimized case. A comparison between the amount of natural gas consumed is reported in FIGURE 19 which proves that although the amount of hydrogen fuel produced and consumed in optimized operation is considerably lower than in the condition-based scenario, the amount of natural gas consumed is lower and in sum the micro gas turbine operated less. The amount of hydrogen produced during day 2 was consumed on day 3 in the optimized operation, which reduced the cost of micro gas turbine operation during day 3 and in comparison with the optimized operation of MG without the electrolyzer.

An overview of total fuel consumption for all studied scenarios is provided in TABLE 5. The amount of natural gas consumed with condition-based operation is about 380 kg higher than the optimized operation in the case of MG with the electrolyzer. Without the electrolyzer, the optimizer consumes about 370 kg less natural gas than the condition based. Looking at the total power produced by the MGT it seems that the optimizer controls the MG in a way that MGT has to operate less and consume less fuel. Note that during the first two days of the week, the MGT power is negative, this is because, below 5 kW of power demand, the MGT works as a consumer to avoid turning off. This was considered during the optimization to avoid repeated shutdowns and startups and cold restarts of the engine which has destructive effect on its lifetime. The consumed fuel is to run the MGT at minimum load and prevent its components from cooling down. However, no load in two consecutive days was foreseen. The engine could be shut down during these days and it will improve the results as MGT is working as a consumer, especially since only keeping the MGT warm is consuming up to 120 kg of natural gas consumption (FIGURE 19, day 1, optimized operations).

TABLE 5: MGT POWER AND FUEL CONSUMPTION OVER THE WEEK.

	Condition-based Operation			Optimized Operation		
Case	H_2 Con. [kg]	NG Con. [kg]	P_{MGT} [MW]	H_2 Con. [kg]	NG Con. [kg]	P_{MGT} [MW]
MG w ELZ	24.03	944.41	2.12	1.56	555.63	0.23
MG w/o ELZ	0	1009.66	2.12	0	636.85	0.75

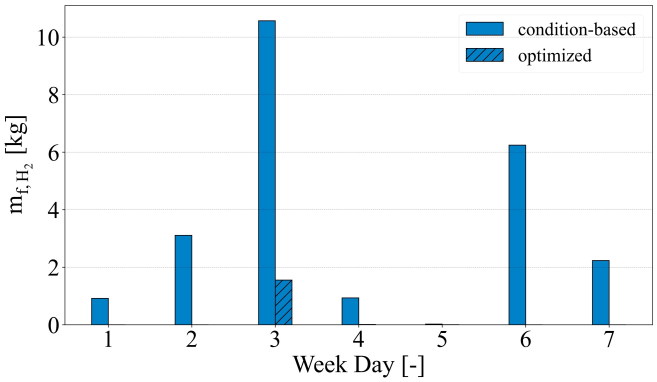

FIGURE 17: HYDROGEN FUEL CONSUMED BY THE MGT OVER THE WEEK.

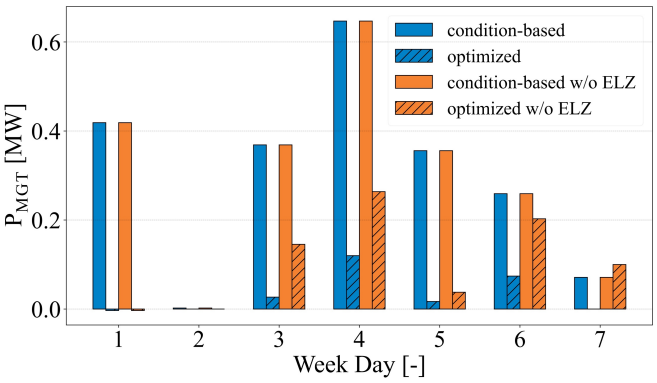

FIGURE 18: POWER PRODUCED BY THE MICRO GAS TURBINE OVER THE WEEK.

The power balance inside the microgrid for each day is depicted in FIGURE 20. Positive values indicate that the production of power inside the microgrid was higher than the MG demand and the excess power is exported (sold) to the grid. Negative values indicate that power has been imported (bought) to the microgrid as the resources inside did not cover the demand. This demand includes both the consumer and the electrolyzer.

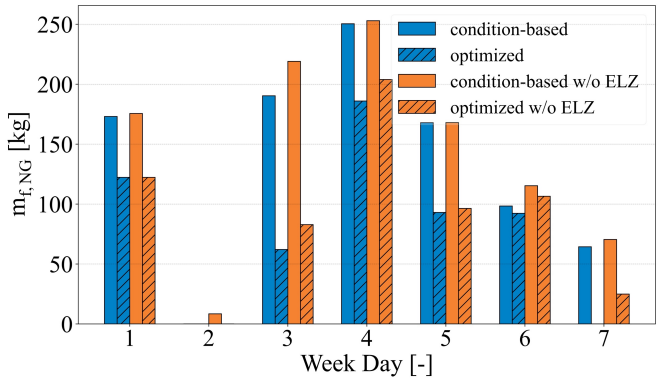

FIGURE 19: NATURAL GAS FUEL CONSUMED BY THE MGT OVER THE WEEK.

The power balance for condition-based operation with an electrolyzer being present is close to zero on all days. When there is no electrolyzer, the chance of exporting power is higher, as occurred on days 1, 2, 5, 6, and 7 according to FIGURE 20. This happened when the wind turbine power is higher than the power demand and heat demand (FIGURE 10). It is also notable that although the total power demand plus heat demand for day 1 is higher than the wind power (FIGURE 15), the operation is conducted on hourly bases and has led to such results. To elaborate, the power balance throughout day 1 of the microgrid running without the electrolyzer is depicted in FIGURE 21.

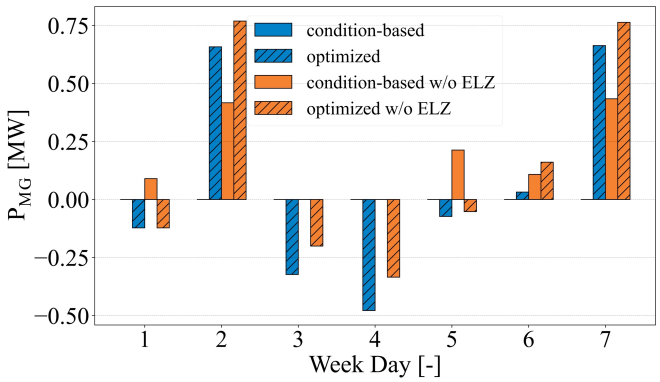

FIGURE 20: POWER BALANCE OF THE MICROGRID OVER THE WEEK.

Another observation from the microgrid power balance is that optimizer operation decided on exporting power on days 2 and 7 for both microgrid configurations, and also on day 6 for no electrolyzer configuration. The main reason is the surplus of wind power on days 2 and 7 that the optimizer decides to sell to the grid for profit. It is worth mentioning that an alternative choice for the optimizer was to use the excess power for water electrolysis to save for hydrogen (similar to condition-based) for the next days which may be prone to low power income from the wind. However, the optimizer is not able to conduct in such a manner since the optimization is confined to 24 hours of operation only, and aims to maximize the economical benefit of only that day. To improve the results, one can increase the window of optimization, but the computational cost for even 2 days is several times higher than 1 day due to the curse of dimensionality. Another way is to modify the hydrogen saving incentives (Eq. 14) to influence the optimizer for dividing the excess power into export and storage, and then overview the results for the whole week to decide how much incentive should be used for hydrogen saving. The produced amount of hydrogen is reported in FIGURE 22. The optimizer realized that on day 2 running the electrolyzer is beneficial. This was anticipated as the wind turbine power was higher than the demanded power and heat (FIGURE 15), however, on day 7 decided to export all the excess power from the wind.

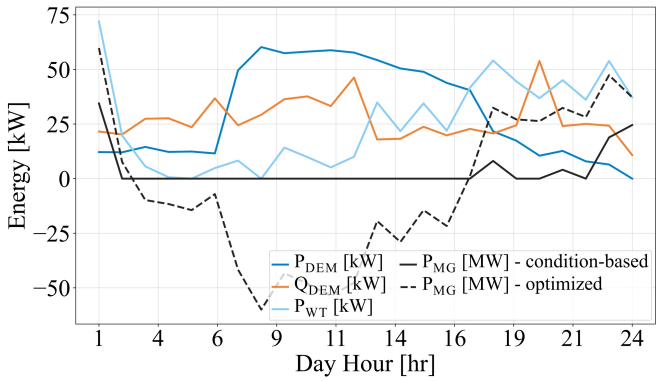

FIGURE 21: THE POWER BALANCE OVER DAY 1 FOR THE MICROGRID WITHOUT ELECTROLYZER.

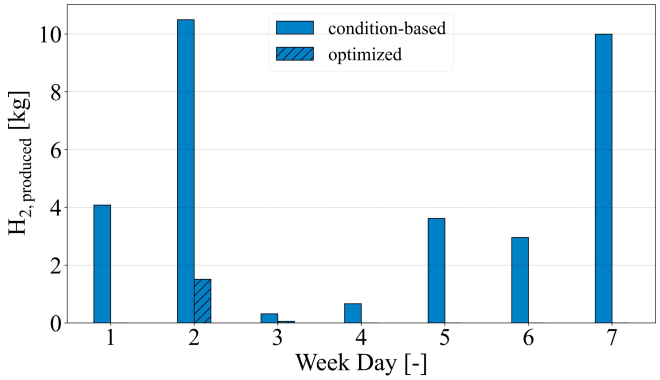

FIGURE 22: PRODUCED AMOUNT OF HYDROGEN OVER THE WEEK.

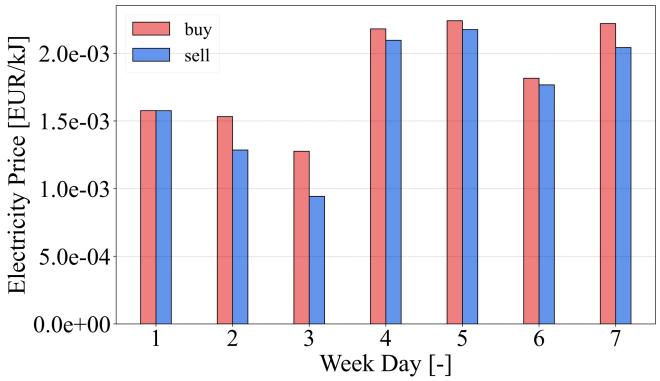

FIGURE 23: ELECTRICITY PRICE DIFFERENCE OVER THE WEEK.

Another observation from the results is the performance of the optimizer in terms of balancing between importing power and running the micro gas turbine. For instance, during day 1, the power required for the microgrid is imported (FIGURE 20) rather than running the micro gas turbine (FIGURE 18). One reason could be the price condition on each day, depicted in FIGURE 23. The price of buying and selling electricity is equal on day 1, so, buying electricity would be beneficial. On day 7 however, the difference is higher, and exporting electricity will be advantageous.

6. CONCLUSION

The operation of a microgrid composed of a wind turbine power generator as the main source of power generation and a fuel flexible micro gas turbine running with blended methane/hydrogen fuel is investigated for optimization. A water electrolyzer and hydrogen tank are present inside the microgrid to operate as a storage system. The operation of the microgrid was studied with and without the electrolyzer connected to the circuit to evaluate the influence of hydrogen storage. Two scenarios were conducted for each configuration: condition-based and optimized. The condition-based scenario works based on power and heat balance inside the microgrid. The optimization scenario, on the other hand, seeks for highest economical results by controlling the dispatchable units inside the microgrid; i.e. the micro gas turbine and the electrolyzer. All of the components of the microgrid are modeled by artificial neural networks based on real operational data, which provided a fast-responding model with accurate results.

The study was conducted in hourly bases for 24 hours of optimization window. Optimization was performed 7 times to complete a study of a week. A summary of the results for the selected a week is presented as follows:

- Optimization of operation reduced the expense of operation by 57% in comparison to condition-based, in the case of electrolyzer present. In the configuration without the electrolyzer 42% of the loss was saved.
- The optimized operation of the microgrid with electrolyzer reduced the loss by 11% compared to the optimized operation without the electrolyzer and hydrogen storage.
- The optimized scenario reduced the consumption of natural gas fuel by 41% for a week of operation, for the configuration with electrolyzer. For the configuration without the electrolyzer 37% of natural gas was saved. Lower natural gas consumption improves both the economical and environmental outcomes of the microgrid.
- The amount of hydrogen produced and consumed in condition-based operation was higher than in optimized operation. However, the optimized scenario had an environmentally more suitable operation as it managed to run the microgrid with lower power of micro gas turbine which led to less fuel, natural gas as well as hydrogen.
- The pricing situation for electricity could affect the optimized operation and making a decision towards balancing, importing, or exporting power. The condition-based scenario operates regardless of the information about pricing and therefore oversees the potential.

ACKNOWLEDGEMENTS

This project has received funding from the European Union's Horizon 2020 research and innovation program under the Marie Skłodowska-Curie grant agreement No. 861079.

REFERENCES

[1] International Energy Agency, "Global Energy & CO2 Status Report - The latest trends in energy and emissions in 2018," 2019. Available: www.iea.org/t&c/

[2] P. Seljom et al., "Modelling the effects of climate change on the energy system—A case study of Norway," Energy Policy, vol. 39, no. 11, pp. 7310–7321, Nov. 2011, doi: 10.1016/J.ENPOL.2011.08.054.

[3] D. Chen, M. C. Facchini, D. Frame, N. Mahowald, and J.-G. Winther, "Introduction," in Climate Change 2013: The Physical Science Basis, Y. Ding, L. Mearns, and P. Wadhams, Eds. Cambidge, United Kingdom: Cambridge University Press, 2013, pp. 119–158.

[4] International Energy Agency, "Global CO2 emissions in 2019 – Analysis - IEA," Feb. 2020. Available: https://www.iea.org/articles/global-co2-emissions-in-2019

[5] A. Kempenaar, E. Puerari, M. Pleijte, and M. van Buuren, "Regional design ateliers on 'energy and space': systemic transition arenas in energy transition processes," European Planning Studies, vol. 29, no. 4, pp. 762–778, 2021, doi: 10.1080/09654313.2020.1781792.

[6] R. Wallsgrove, J. Woo, J. H. Lee, and L. Akiba, "The Emerging Potential of Microgrids in the Transition to 100% Renewable Energy Systems," Energies (Basel), vol. 14, no. 6, p. 1687, Mar. 2021, doi: 10.3390/EN14061687.

[7] A. Hirsch, Y. Parag, and J. Guerrero, "Microgrids: A review of technologies, key drivers, and outstanding issues," Renewable and Sustainable Energy Reviews, vol. 90, pp. 402–411, Jul. 2018, doi: 10.1016/J.RSER.2018.03.040.

[8] M. F. Roslan, M. A. Hannan, P. J. Ker, K. M. Muttaqi, and T. M. I. Mahlia, "Optimization algorithms for energy storage integrated microgrid performance enhancement," J Energy Storage, vol. 43, p. 103182, Nov. 2021, doi: 10.1016/J.EST.2021.103182.

[9] Y. Parag and M. Ainspan, "Sustainable microgrids: Economic, environmental and social costs and benefits of microgrid deployment," Energy for Sustainable Development, vol. 52, pp. 72–81, Oct. 2019, doi: 10.1016/J.ESD.2019.07.003.

[10] M. F. Akorede, H. Hizam, and E. Pouresmaeil, "Distributed energy resources and benefits to the environment," Renewable and Sustainable Energy Reviews, vol. 14, no. 2, pp. 724–734, Feb. 2010, doi: 10.1016/J.RSER.2009.10.025.

[11] “Microgrids - Part 1: Guidelines for microgrid projects planning and specification,” May 2017.
[12] J. M. Raya-Armenta, N. Bazmohammadi, J. G. Avina-Cervantes, D. Sáez, J. C. Vasquez, and J. M. Guerrero, “Energy management system optimization in islanded microgrids: An overview and future trends,” Renewable and Sustainable Energy Reviews, vol. 149, p. 111327, Oct. 2021, doi: 10.1016/J.RSER.2021.111327.
[13] S. Khan, D. Paul, P. Momtahan, and M. Aloqaily, “Artificial Intelligence Framework for Smart City Microgrids: State of the art, Challenges, and Opportunities,” in 2018 Third International Conference on Fog and Mobile Edge Computing (FMEC) , 2018.
[14] P. García, J. P. Torreglosa, L. M. Fernández, and F. Jurado, “Optimal energy management system for stand-alone wind turbine/photovoltaic/hydrogen/battery hybrid system with supervisory control based on fuzzy logic,” Int J Hydrogen Energy, vol. 38, no. 33, pp. 14146–14158, Nov. 2013, doi: 10.1016/J.IJHYDENE.2013.08.106.
[15] M. F. Roslan, M. A. Hannan, P. J. Ker, K. M. Muttaqi, and T. M. I. Mahlia, “Optimization algorithms for energy storage integrated microgrid performance enhancement,” J Energy Storage, vol. 43, p. 103182, Nov. 2021, doi: 10.1016/J.EST.2021.103182.
[16] M. Marinelli, F. Sossan, G. T. Costanzo, and H. W. Bindner, “Testing of a predictive control strategy for balancing renewable sources in a microgrid,” IEEE Trans Sustain Energy, vol. 5, no. 4, pp. 1426–1433, Oct. 2014, doi: 10.1109/TSTE.2013.2294194.
[17] F. Mohamed, “MICROGRID MODELLING AND SIMULATION,” Helsinki University of Technology , Otaniemi, 2006.
[18] O. Abrishambaf, P. Faria, L. Gomes, J. Spínola, Z. Vale, and J. M. Corchado, “Implementation of a Real-Time Microgrid Simulation Platform Based on Centralized and Distributed Management,” Energies (Basel), vol. 10, no. 6, p. 806, Jun. 2017, doi: 10.3390/EN10060806.
[19] R. Banihabib, M. J. Obrist, M. Assadi, and P. Jansohn, “Micro Gas Turbine Modelling And Adaptation For Condition Monitoring,” in Global Power and Propulsion, 2022.
[20] R. Banihabib and M. Assadi, “The Role of Micro Gas Turbines in Energy Transition,” Energies (Basel), vol. 15, no. 21, p. 8084, Oct. 2022, doi: 10.3390/EN15218084.
[21] A. Y. Alanis, N. Arana-Daniel, and C. Lopez-Franco, Eds., Artificial Neural Networks for Engineering Applications. Mara Conner, 2019.
[22] “The three point project Triangulum.” https://triangulum-project.eu
[23] “Norwegian Standard 3031:2014 Calculation of energy performance of buildings — Method and data, appendix b.”
[25] R. Banihabib and M. Assadi, “A Hydrogen-Fueled Micro Gas Turbine Unit for Carbon-Free Heat and Power Generation,” Sustainability, vol. 14, no. 20, p. 13305, Oct. 2022, doi: 10.3390/SU142013305.
[26] “Fraunhofer ISE—Annual Report 2020/2021 ,” Freiburg, Germany, 2021.
[27] A. K. Shaikh, A. Nazir, I. Khan, and A. S. Shah, “Short term energy consumption forecasting using neural basis expansion analysis for interpretable time series,” Sci Rep, vol. 12, no. 1, pp. 1–18, Dec. 2022, doi: 10.1038/s41598-022-26499-y.
[28] “RME - The Regulatory Authority for Energy.” https://www.nve.no/reguleringsmyndigheten/
[29] S. Jin, S. Wang, and F. Fang, “Game theoretical analysis on capacity configuration for microgrid based on multi-agent system,” International Journal of Electrical Power & Energy Systems, vol. 125, p. 106485, Feb. 2021, doi: 10.1016/J.IJEPES.2020.106485.
[30] P. Virtanen et al., “SciPy 1.0: fundamental algorithms for scientific computing in Python,” Nature Methods 2020 17:3, vol. 17, no. 3, pp. 261–272, Feb. 2020, doi: 10.1038/s41592-019-0686-2.